CONF-900557--1

CONF-900557--1

DE90 010434

The ATF Two-Frequency Correlation Reflectometer*

G. R. Hanson,[a] J. B. Wilgen, E. Anabitarte,[b] J. D. Bell,[c] J. H. Harris, J. L. Dunlap, and C. E. Thomas[a]

Oak Ridge National Laboratory
Oak Ridge, Tennessee 37831-8072

*Research sponsored by the Office of Fusion Energy, U.S. Department of Energy, under contract DE-AC05-84OR21400 with Martin Marietta Energy Systems, Inc., and by the Asociación EURATOM/CIEMAT, Madrid, Spain.

[a]Permanent address: Georgia Institute of Technology, Atlanta, Georgia.

[b]Permanent address: Asociación EURATOM/CIEMAT, Madrid, Spain.

[c]Computing and Telecommunications Division, Martin Marietta Energy Systems, Inc.

The ATF two-frequency correlation reflectometer*

G. R. Hanson[a)], J. B. Wilgen, E. Anabitarte[b)], J. D. Bell[c)], J. H. Harris, J. L. Dunlap, and C. E. Thomas[a)]

Fusion Energy Division, Oak Ridge National Laboratory, Oak Ridge, Tennessee 37831-8072

The Advanced Toroidal Facility (ATF) density fluctuation reflectometer system consists of two individual reflectometers operating in the 30- to 40-GHz band. Each reflectometer consists of a tunable microwave source and a quadrature phase detector connected to the same antenna system. This arrangement allows two-frequency operation along the same radial chord for radial coherence measurements.

The technique used in making radial coherence measurements is discussed and the results of such experiments are given. Initial experiments have shown high coherence when the frequencies of the two reflectometers are tuned close together and a clear loss of coherence as the radial separation of the cutoff layers is increased by increasing the frequency separation of the two reflectometers.

Recent results have shown that local measurements of density fluctuations in plasmas with electron cyclotron heating (ECH) are possible and that detailed structure can been seen in the fluctuation spectra. In addition, radial correlation lengths have been found to be from 0.5 to 1.0 cm in ECH plasmas, with some frequency structures having correlation lengths up to 3 cm. In plasmas with neutral beam injection (NBI), the radial correlation lengths in the edge region have been found to be approximately 0.1–0.2 cm.

I. SYSTEM DESCRIPTION

The ATF reflectometer operates two frequencies simultaneously in the same antenna system. Two tunable microwave sources allow continuous operation between 30 and 40 GHz with separation frequencies from 10 MHz to 10 GHz. The antenna system consists of two high-gain (27 dB average) conical horns with a predicted spot size at the mean reflecting layer of 6 cm at 35 GHz. The horns are located on the horizontal midplane with an angle of 12° relative to one another with their apertures located at $R = 2.70$ m ($R_0 = 2.10$ m, $a = 0.28$ m) so that their sightlines cross at $r/a \simeq 0.75$. This position is defined as the mean reflecting layer.

Figure 1 shows the basic components and their position in the reflectometer system. The antennas are located inside the vacuum vessel with waveguide windows at the vacuum interface. The dual antenna arrangement greatly reduces the effects of internal reflections in the waveguide system (as compared to a single antenna system). The waveguide vacuum windows are 0.0035-in.-thick mica disks sealed with O-rings at the vacuum interface waveguide joint. Transition to circular waveguide is made outside the vacuum windows to allow launching of any arbitrary orientation of wave electric field. Rectangular waveguide twists connected to the circular transitions are used to match the waveguide polarization to the desired antenna polarization for launching either the ordinary mode (O-mode) or the extraordinary mode (X-mode). Low-pass filters with >35-dB rejection above 47 GHz are used to eliminate interference from the 53-GHz electron cyclotron resonant heating frequency.

Quadrature phase detection (or balanced dual-homodyne detection) is used to measure the phase fluctuations in the reflected signal. Quadrature phase detection is obtained using two balanced detectors with a 90° phase relation. The inset in Fig. 1 shows the quadrature phase detector. Each balanced detector consists of two crystal detectors and a 3-dB 90° hybrid coupler. Balanced detection is achieved by combining the outputs from these detectors in a differential amplifier. Two more 3-dB 90° hybrid couplers are used to divide and direct the reflected and reference signals to the two balanced detectors. Two $\lambda_g/8$ waveguide spacers inserted between the balanced detectors provide the 90° phase delay for quadrature detection. The differential amplifiers are a three-stage, low noise design with a variable gain factor up to 1000 and a 3-dB bandwidth of 225 kHz. A resistive divider circuit at each amplifier input allows balancing of the signals from each detector pair to remove any dc offset remaining after differential amplification. Anti-aliasing filtering is used with the filter cutoff frequency usually set to 60–80% of the Nyquist frequency. After anti-aliasing filtering, the signals are digitized in a transient recorder with 16 kbytes/channel of memory.

Quadrature phase detection is a type of homodyne detection that is superior to simple homodyne detection because it provides the two output signals $S_a = \tilde{A}\sin\tilde{\zeta}$ and $S_b = \tilde{A}\cos\tilde{\zeta}$, where $\tilde{\zeta}$ is the phase fluctuation in the reflected signal resulting

from fluctuations in the critical layer, and $\bar{A}$ is the fluctuating amplitude of the reflected signal. The fluctuating amplitude can be calculated from $\bar{A} = (S_a^2 + S_b^2)^{1/2}$ and removed from S_a and S_b to obtain $\sin\bar{\zeta}$ and $\cos\bar{\zeta}$. S_a and S_b can also be used in a fringe counting program to calculate the actual phase fluctuations; however, it is common for up to 1% of the data points to result in fringe skips, significantly distorting the low-frequency end of the power spectrum. If manual correction of the fringe skips is used, the high-frequency end of the spectrum is distorted. In practice, the signals $\sin\bar{\zeta}$ and $\cos\bar{\zeta}$ are analyzed on a regular basis, and fringe counting is used when the amplitude of a particular phase fluctuation is desired.

A difficulty that arises when analyzing the data is that each quadrature phase detector is designed for a specific center frequency, and at other frequencies, S_a and S_b do not have a 90° phase relation. However, the amount of phase deviation $\Delta\psi$ can be measured, and S_b can be advanced or delayed using the relationship

$$S_b' = \frac{S_b - S_a \sin(\Delta\psi)}{\cos\Delta\psi} \tag{1}$$

to obtain a 90° phase relation between S_a and S_b'.

Two-frequency operation is achieved by combining and dividing the transmitted and reflected signals in two 3-dB couplers. Independent detection of the two signals with a frequency separation as low as 10 MHz is possible because of the homodyne detection. If two reflected signals with frequencies f_1 and f_2 are mixed with the f_1 reference signal at a crystal detector (purity of the reference signal is critically important), two IF signals are possible. The first will have a zero IF, while the second will have a frequency of $|f_1 - f_2|$. Since the crystal detectors have a bandwidth of only 400 kHz, only the zero IF signal, which contains the phase and amplitude fluctuations from the f_1 reflected signal, can be detected. The f_1 detector's response to the power fluctuations of the f_2 reflected signal is negligible compared to the detector's response to the f_1 signal's phase and amplitude fluctuations; thus, the fluctuations in the f_2 signal are invisible to the f_1 detection system. This is a result of the vector addition of the amplitudes of the f_1 reference and reflected signals at the detector (as long as the detector is operating in the square-law regime) and of the reference signal power being approximately 20 dB higher than the reflected signal power.

The vector addition of the amplitudes rather than the simple addition of the powers also greatly improves the signal-to-noise ratio. The two largest noise sources are the amplifiers and the microwave sources. In both cases, the noise levels are 20 dB below the normal plasma signal level for frequencies in the range of above 5 kHz to 100 kHz.

The plasma regimes that can be studied are limited because of the small rf frequency band of the reflectometer. The density range that can be studied in ATF with a 30- to 40-GHz reflectometer is limited to 1.1–2.0 $\times$ 10^{13} cm^{-3} for O-mode operation and to approximately 1.5–8.5 $\times$ 10^{12} cm^{-3} for X-mode operation at 0.95 T.

X-mode operation at 1.9 T is not useful because the cutoff occurs on the low-field side of the fundamental cyclotron resonance (well outside the last closed flux surface). For X-mode operation, low-density ECH discharges can be studied over most of the minor radius for near-parabolic density profiles; however, since ATF often has nearly flat profiles, the reflecting layer is often restricted to the outer third of the plasma. For O-mode operation, NBI plasmas are studied; however, the much higher density of these discharges limits the measurement to the edge of the plasma. A higher frequency system operating between 65 and 85 GHz is planned for the future to allow internal probing of NBI plasmas.

II. RADIAL COHERENCE MEASUREMENTS

The capability of the ATF reflectometer to operate two frequencies simultaneously along the same radial chord with a frequency separation as low as 10 MHz provides a simple means of making radial coherence measurements. The frequency-resolved coherence $\gamma(f)$ between the signals reflected at the two critical layers is calculated using standard cross-correlation techniques and is determined as a function of the frequency separation of the two signals. Conversion to a radial distance is dependent on knowing the density gradient. It has been found that for coherence measurements, the amplitude fluctuations in the reflected signal have only a minor effect on the coherence.

A difficulty that arises in the determination of the coherence is that the signals to be analyzed are the sine and cosine of a phase fluctuation $\tilde{\zeta}$. The normalized coherence between two signals $\sin(\tilde{\zeta}_1)$ and $\sin(\tilde{\zeta}_2 + \varphi)$ is approximately equal to $\langle \tilde{\zeta}_1 \tilde{\zeta}_2 \rangle |\cos\varphi|$, where the angle brackets $\langle\ \rangle$ indicate the coherence from the cross-correlation of $\tilde{\zeta}_1$ and $\tilde{\zeta}_2$. Thus for $\varphi = 0°$, the coherence is maximum, while for $\varphi = 90°$ the coherence is a minimum.

In the case of radial coherence measurements between two cutoff layers, the two signals to be analyzed are $\sin\tilde{\zeta}_1$ and $\sin(\tilde{\zeta}_2 + \varphi)$, where φ is a phase delay between the two signals resulting from the difference in the propagation path lengths. For two simple homodyne detection systems, $|\varphi|$ can vary from 0° to 90°, and the apparent coherence between the two detector signals can be much less than the true coherence. If one of the reflectometer frequencies is scanned continuously away from the other frequency, then the coherence will vary sinusoidally between the true coherence and zero as a function of the separation frequency.

For quadrature phase detection, the two signals to be analyzed are selected from the four signals

$$V_1 = \tilde{A}_1 \begin{Bmatrix} \sin \\ \cos \end{Bmatrix} \tilde{\zeta}_1 \quad ,$$

$$V_2 = \tilde{A}_2 \begin{Bmatrix} \sin \\ \cos \end{Bmatrix} \tilde{\zeta}_2 + \varphi \quad ,$$

where V_1 and V_2 are from the first and second reflectometers, respectively, and two signals can be selected such that $|\varphi| \leq 45°$. The coherence between V_1 and V_2 is calculated as a time average over 127 realizations for a 32-ms data window (16 kbytes of data at a sampling speed of 512 kHz). The cross-correlation calculation determines $\gamma(f)$ and the phase relation (as long as there is coherence) between the two signals. For a given frequency separation of the two reflectometers, only the two signals producing the maximum coherence are used. In the worst case, φ could be 45°, which corresponds to an error in γ of 30%. Radial coherence plots (such as Fig. 2) are obtained using this type of data selection.

Figure 2 shows a plot of the radial coherence of the density fluctuations measured by the reflectometers vs the separation frequency of the two probing beams in the edge of an NBI plasma. The coherence length is estimated, using the density profile obtained by Thomson scattering, to be approximately 0.1–0.2 cm. The lack of a precise knowledge of the radial density gradient represents the primary source of error in quoting the coherence length, as the uncertainty in the Thomson scattering data is large. The radial position of the cutoff layer is at $r/a \simeq 1.1$. The radial coherence length in ECH plasmas has been found to be about 0.5–1.0 cm with some fluctuation peaks (such as those in Fig. 3) having coherence lengths up to 3 cm. Thomson scattering profiles indicate the position of the cutoff layers in this case to be between $r/a \simeq 0.85$ and $r/a \simeq 0.95$. The fact that the coherence decreases rapidly as the frequency separation is increased is evidence of the localization of the measurement.

III. DENSITY FLUCTUATION SPECTRA

Reflectometry allows internal probing of the plasma to measure the density fluctuation spectra. Although exact determination of $\tilde{n}/n$ is difficult, localized measurements of features in the fluctuation spectrum are possible. Figure 3 shows a fluctuation power spectrum obtained with the reflectometer in an ECH plasma. This spectrum was obtained from the signal $\cos\tilde{\zeta}$, where $\tilde{\zeta}$ is related to $\tilde{n}_e$. The two large structures at 20 kHz and 40–60 kHz have radial coherence lengths of about 1.0 cm and 3.0 cm, respectively. As the cutoff layer is scanned farther inward, the peaks begin to decrease and finally disappear. Figure 4 shows the spectrum for a radial position approximately 0.5–1.0 cm farther into the plasma.

*Research sponsored by the Office of Fusion Energy, U.S. Department of Energy, under contract DE-AC05-84OR21400 with Martin Marietta Energy Systems, Inc., and by the Asociación EURATOM/CIEMAT, Madrid, Spain.

[a]Georgia Institute of Technology, Atlanta, GA.

[b]Asociación EURATOM/CIEMAT, Madrid, Spain.

[c]Computing and Telecommunications Division, Martin Marietta Energy Systems, Inc.

Figure 1: Diagram of the ATF reflectometer system showing the major components.

Figure 2: Radial coherence of density fluctuations in the edge of an NBI plasma.

Figure 3: Fluctuation power spectrum in an ECH plasma obtained by reflectometry, showing large frequency structure at 20 kHz and 40–60 kHz.

Figure 4: Fluctuation power spectrum for a radial position farther inside the plasma than that in Fig. 3 in the same ECH sequence.

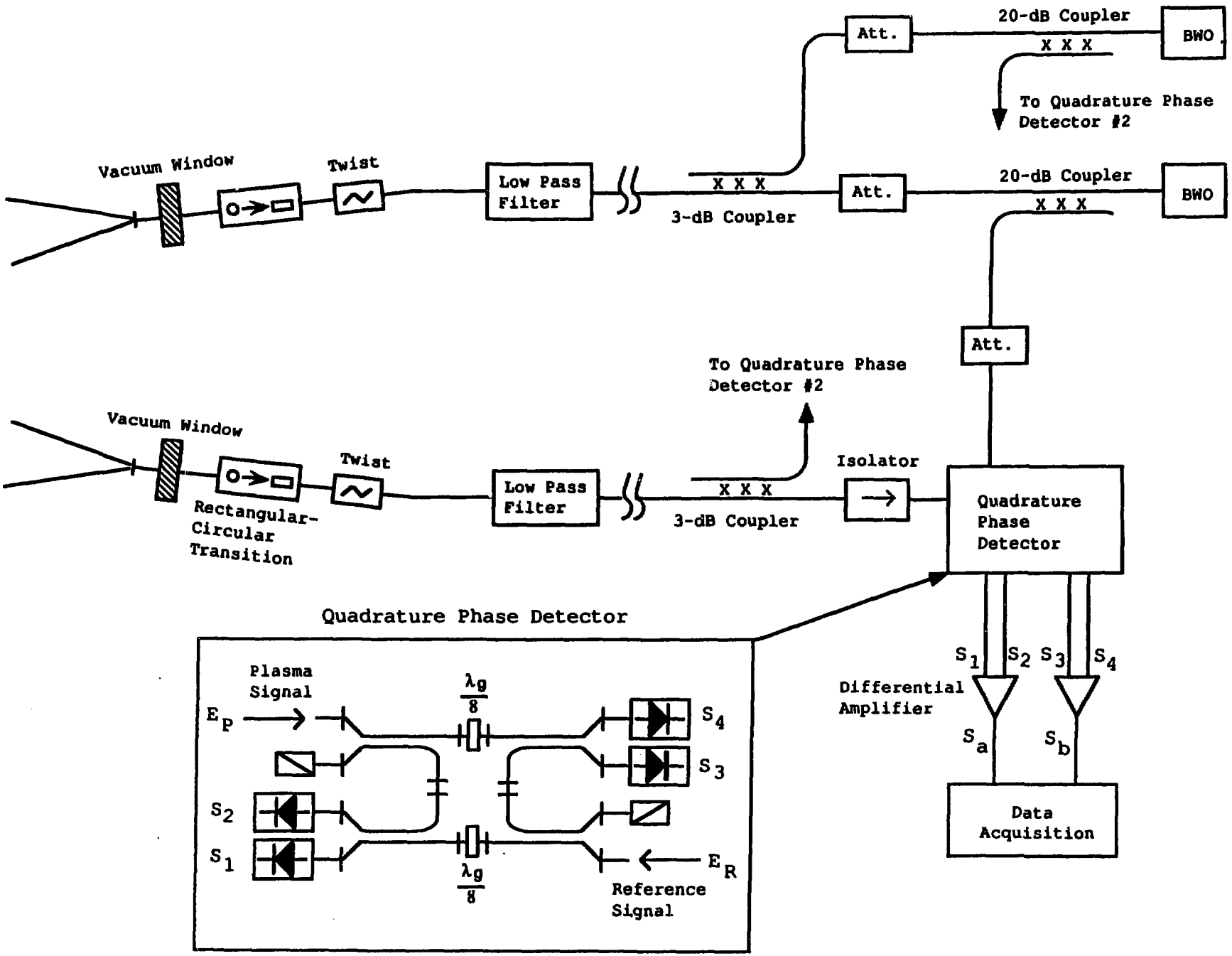
Att.
20-dB Coupler
BWO
X X X
To Quadrature Phase Detector #2
Vacuum Window
Twist
Low Pass Filter
X X X
3-dB Coupler
Att.
20-dB Coupler
BWO
X X X
Att.
To Quadrature Phase Detector #2
Vacuum Window
Twist
Isolator
Rectangular-Circular Transition
Low Pass Filter
X X X
3-dB Coupler
Quadrature Phase Detector
Quadrature Phase Detector
Plasma Signal
E_P
$\frac{\lambda g}{8}$
S_4
S_3
S_2
S_1
$\frac{\lambda g}{8}$
E_R
Reference Signal
S_1 S_2 S_3 S_4
Differential Amplifier
S_a
S_b
Data Acquisition

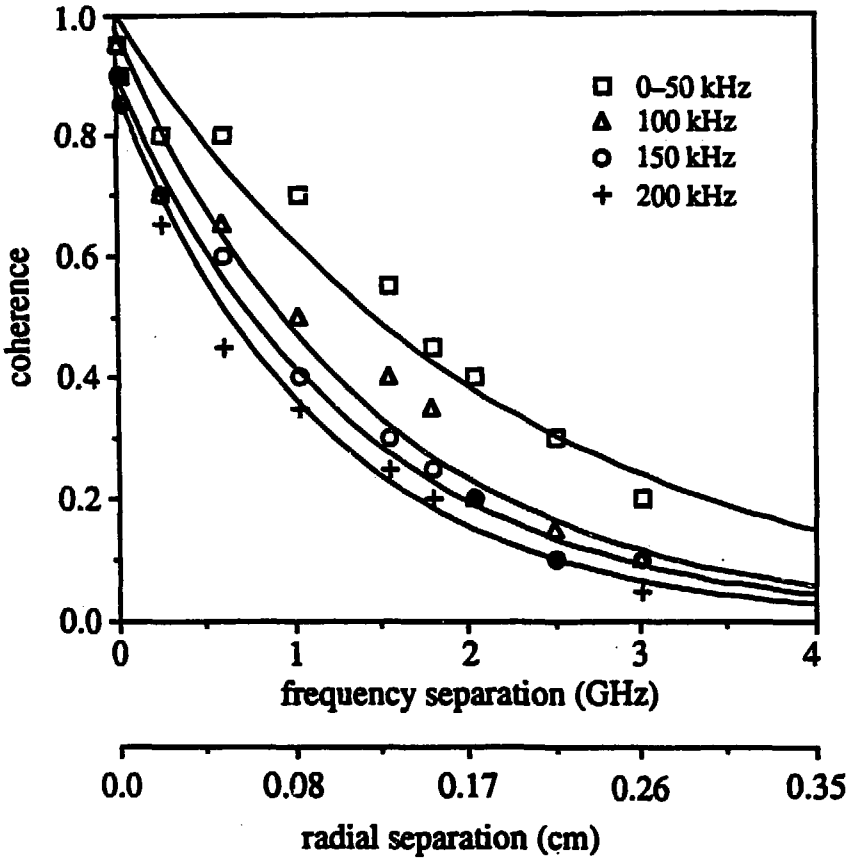
1.0
0.8
0.6
0.4
0.2
0.0
coherence
0–50 kHz
100 kHz
150 kHz
200 kHz
0
1
2
3
4
frequency separation (GHz)
0.0
0.08
0.17
0.26
0.35
radial separation (cm)

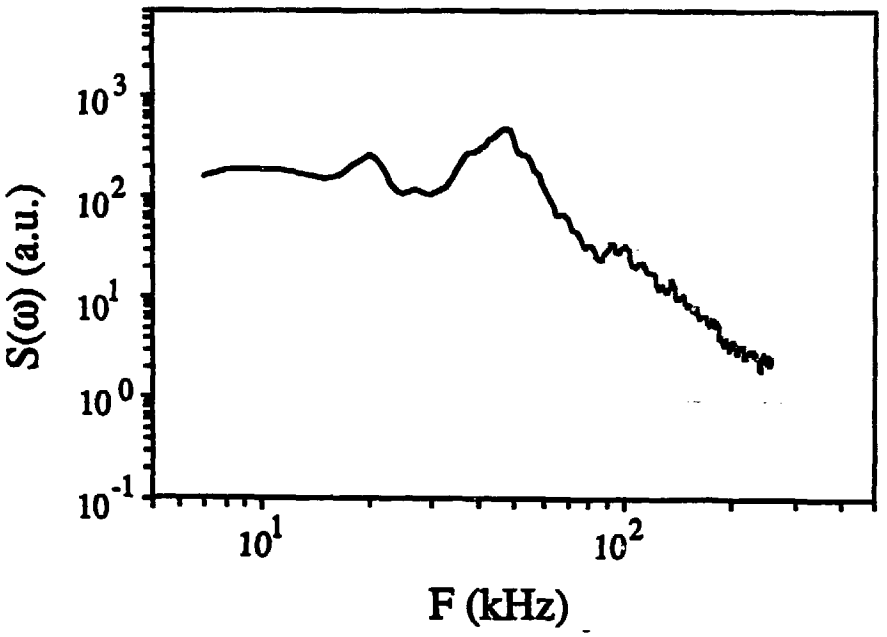
10^3
10^2
10^1
10^0
10^{-1}
S(ω) (a.u.)
10^1
10^2
F (kHz)

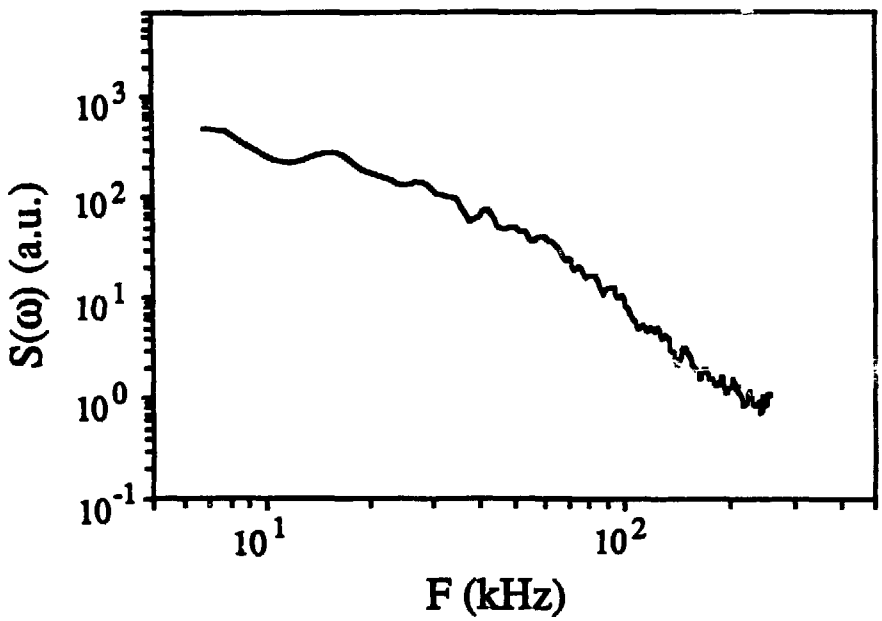
S(ω) (a.u.)
10^3
10^2
10^1
10^0
10^-1
10^1
10^2
F (kHz)